

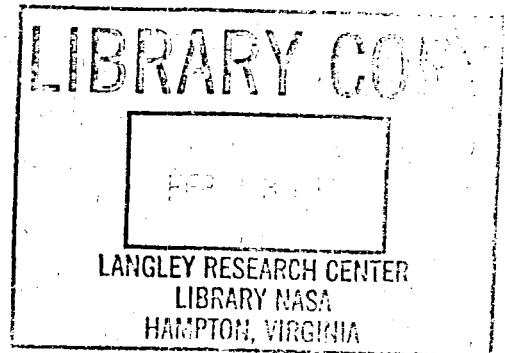
**NASA
Technical
Paper
3162**

January 1992

NASA-TP-3162 19920007852

High-Temperature Durability Considerations for HSCT Combustor

Nathan S. Jacobson



NASA

**NASA
Technical
Paper
3162**

1992

High-Temperature Durability Considerations for HSCT Combustor

Nathan S. Jacobson
*Lewis Research Center
Cleveland, Ohio*



National Aeronautics and
Space Administration
Office of Management
Scientific and Technical
Information Program

Summary

The novel combustor designs for the High Speed Civil Transport will require high-temperature materials with long-term environmental stability. Higher liner temperatures than in conventional combustors and the need for reduced weight necessitate the use of advanced ceramic-matrix composites. In this report the combustor environment is defined at the current state of design, the major degradation routes are discussed for each candidate ceramic material, and where possible, the maximum use temperatures are defined for these candidate ceramics.

Introduction

A key issue in the development of a viable High Speed Civil Transport (HSCT) is the necessity to produce a combustor that minimizes nitrogen oxide (NO_x) emissions (ref. 1). Three combustor concepts are currently under consideration: (1) rich burn/quick quench/lean burn (RQL), (2) lean premixed/prevaporized (LPP), and (3) rich-zone variant catalytic oxidation. These concepts are illustrated in figure 1. The primary emphasis of this report is on materials considerations for the first two designs, but some of the conclusions are also valid for the catalytic system.

The combustors' environments, especially that of the RQL combustor, are expected to be radically different from those for current combustors. Fuel-rich conditions mean that currently used film cooling from bypass air cannot be utilized. Thus only back-side cooling can be used, and the combustor liner will experience very high temperatures. The actual combustor liner surface temperature is controlled by a number of factors including the flame temperature, which may exceed 2400 K for short times, and the heat transfer characteristics of the combustion gas and liner. Limited film cooling will be possible in the LPP combustor. For both the RQL and LPP combustors high-temperature liner materials are a necessity. In addition, the projected lifetime of the HSCT combustor is approximately 18 000 hr, making long-term environmental durability a critical factor in its development.

In addition to high-temperature durability, candidate combustor liners must offer low density. For these reasons advanced ceramics are the leading candidate materials. The base ceramic materials currently under consideration are

- (1) Nonoxides
 - (a) SiC, Si_3N_4 , MoSi_2 , and AlN
 - (b) Ceramic-matrix composites (CMC's)—SiC (fiber)/SiC (matrix) and SiC (fiber)/ Si_3N_4 (matrix).
- (2) Oxides— Al_2O_3 , $3(\text{Al}_2\text{O}_3) \cdot 2(\text{SiO}_2)$ [mullite], $\text{TiO}_2 \cdot \text{Al}_2\text{O}_3$, $3(\text{Y}_2\text{O}_3) \cdot 5(\text{Al}_2\text{O}_3)$ [YAG], and $\text{Y}_2\text{O}_3 \cdot 2(\text{ZrO}_2)$

In general, the silicon-base materials offer higher thermal conductivities and better mechanical properties than other ceramic systems, but the oxides generally offer better environmental resistance (ref. 2). Materials selection is often a tradeoff between environmental resistance, mechanical properties, and physical properties.

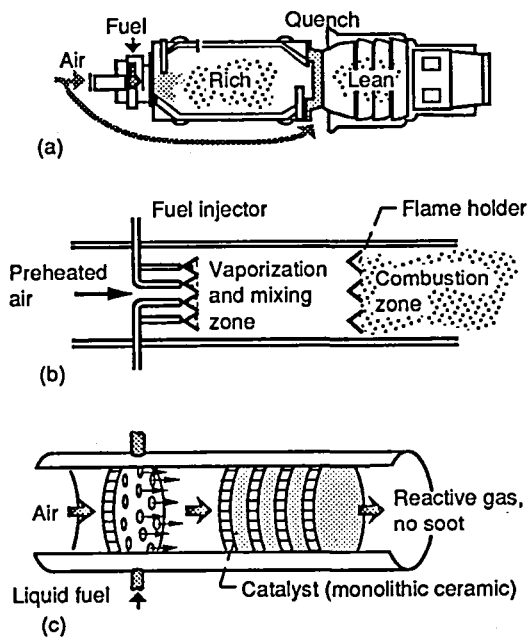
The purposes of this report are threefold: (1) to define the chemical and physical environment of the HSCT combustor at the current state of design, (2) to discuss the major degradation routes of candidate ceramic combustor liners, and (3) to establish maximum use temperatures for each candidate ceramic. The third task is the most difficult, as not all degradation routes can be adequately modeled for each ceramic. Accomplishment of these three tasks should guide materials development for the HSCT combustor.

Combustor Environment

The primary parameters of interest are combustor temperature; combustion gas composition, pressure, and flow velocity; and combustor geometry. The adiabatic flame temperature and combustion gas composition as a function of equivalence ratio and pressure are given in figure 2. The operating regions for the fuel-lean and fuel-rich portions of the RQL combustor are shown. The temperatures and gas compositions were calculated in order to obtain the equilibrium products by using the NASA CEC program (ref. 3), which is a computer code that takes a set of reactants and minimizes the free energy subject to certain constraints. In this case, Jet A fuel ($\text{CH}_{1.9185}$) and air were the reactants. Note that an equivalence ratio of 1 is defined as complete combustion of the fuel to CO_2 and H_2O and that for Jet A fuel (ref. 4)

$$\text{Fuel/air} = 0.068 \times \text{Equivalence ratio} \quad (1)$$

Fuel/air ratio is defined as a weight ratio. Adiabatic conditions were established by setting the net heat flow from the system equal to zero.



- (a) Rich burn/quick quench/lean burn. Burning with excess fuel: equivalence ratio, 1.2 to 1.8; burning with excess air: equivalence ratio, 0.6.
 (b) Lean premixed/prevaporized. Burning with excess air in lean zone: equivalence ratio, 0.6.
 (c) Rich-zone variant catalytic oxidation. Catalytic burning of highly excess fuel: equivalence ratio, 3.0 to 9.0.

Figure 1.—Proposed combustor schemes for HSCT.

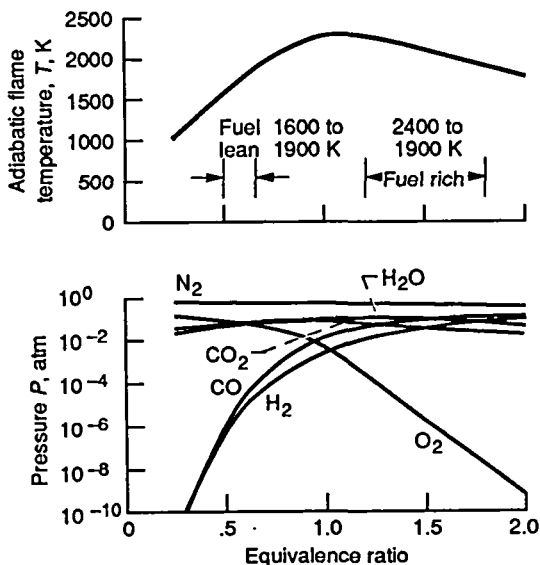


Figure 2.—Calculated adiabatic flame temperature and calculated gas composition as a function of equivalence ratio.

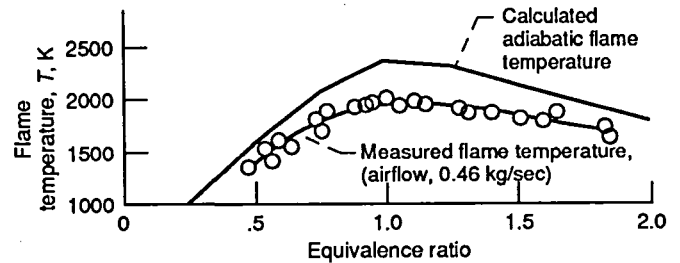


Figure 3.—Calculated adiabatic flame temperature and measured flame temperature in NASA high-pressure burner rig as a function of equivalence ratio. Pressure, 1 atm; fuel, Jet A; water content in air, 1%.

It is important to recognize that the adiabatic flame temperature is a maximum temperature. Figure 3 shows experimental flame temperatures measured on the NASA Lewis Research Center high-pressure burner rig. These temperatures were measured with a thermocouple at the combustor exit. They are lower than the adiabatic flame temperature because of the unavoidable heat losses in any real system. All combustors would be expected to show heat losses, although the degree of loss would be different for each specific system. The temperature of the combustor liner would also be expected to be lower than the adiabatic flame temperature. It is a function of the heat transfer characteristics of the combustor gases and the combustor liner and the extent of cooling. An estimation of this liner surface temperature is beyond the scope of this report.

As mentioned, the gas composition as a function of equivalence ratio is given in figure 2, for a corresponding adiabatic flame temperature. For all equivalence ratios substantial amounts of N_2 and the combustion products CO_2 and H_2O are present. In the fuel-lean region O_2 is present in large amounts. Current gas turbines operate near this region; and many oxidation/corrosion studies have been directed at understanding materials behavior in this type of atmosphere. The fuel-rich atmosphere is less familiar. It consists of large amounts of H_2 and CO . However, the atmosphere is not reducing because the combustion products CO_2 and H_2O can act as oxidants. This is discussed in greater detail in the oxidation section of this report. It is important to recognize that these calculations of combustion products assume equilibrium. Gas compositions will vary if equilibrium is not attained.

The issue of condensed phase deposits is important in current gas turbines. Two types of deposits are sodium vanadate and sodium sulfate. The vanadate deposits form from vanadium impurities in fuels of lower purity than Jet A, so that they are not likely to be an issue. Sodium sulfate (Na_2SO_4) forms from ingested sodium and sulfur impurities in the fuel. Figure 4 shows a plot of calculated dewpoints for Na_2SO_4 at various pressures and sodium levels (ref. 5). In general, the operating temperatures of the HSCT combustor are above these dewpoints, so that Na_2SO_4 deposition may not be an issue. However, if the combustor is operated near a marine environ-

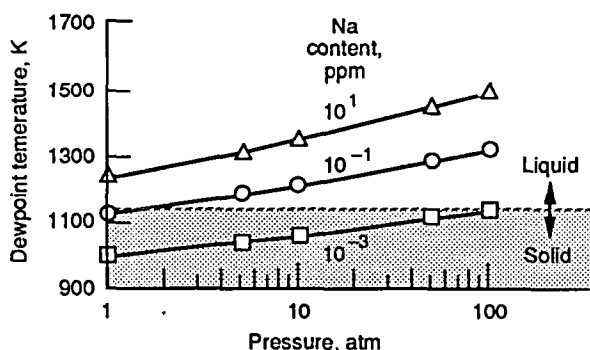


Figure 4.—Calculated dewpoints for Na_2SO_4 deposition. Fuel/air ratio, 0.025; sulfur content, 0.05% (Jet A). From reference 5.

ment (e.g., a coastal runway) that has high sodium levels, Na_2SO_4 may condense on cooler spots in the hot-gas path. Under certain conditions these deposits can be quite corrosive to silicon-base ceramics (ref. 6). In summary, Na_2SO_4 -induced corrosion is not predicted to be an issue in the HSCT combustor. However, it is important to be aware of the conditions under which these deposits may form because they can be quite serious.

The other relevant parameters are pressure, gas velocity, and geometry. The approximate pressure for the suggested combustor designs is 15 atm, with possible maximum pressures of 30 atm. The flow velocities are expected to be about 50 to 100 ft/sec (15.24 to 30.48 m/sec). An annular combustor design is proposed with an outer diameter of about 5 ft (1.52 m) and an inner diameter of about 4 ft (1.22 m). The actual ceramic liner is currently projected to be about 0.1 in. (0.254 cm) thick.

Degradation Routes

The candidate ceramic materials degrade chemically by three major routes: (1) oxidation, (2) vaporization, and (3) interfacial reactions. Each of these is discussed in general terms before proceeding to discussions of the specific materials.

Oxidation

Degradation by oxidation applies only to the nonoxide candidate ceramics. SiC , Si_3N_4 , and MoSi_2 form SiO_2 scales; AlN forms Al_2O_3 . In a fuel-lean environment these oxide scales will form readily. However, even in the fuel-rich environment CO_2 and H_2O act as oxidants and form these oxide scales. The necessary characteristics of a stable, protective oxide scale are

- (1) Dense, effective barrier to oxygen
- (2) Thin and slow growing
- (3) Self-healing in the event of a crack
- (4) Durable in the presence of thermal cycling

- (5) Durable in the presence of secondary compounds, such as water vapor, hydrogen, carbon-containing gases, and sulfur-containing gases

In general, SiO_2 and Al_2O_3 are slow-growing, protective oxides. In dry oxygen and under isothermal conditions both SiO_2 and Al_2O_3 form as thin, protective scales at the temperatures of interest (ref. 2). The difficulty is in extrapolating such data to very long times and to the complex combustor environment of the HSCT. In this environment the scales will be thermally cycled and subjected to the various secondary compounds listed in (5). Inadequate data exist on these effects, and therefore it is not possible to calculate a maximum use temperature for oxidation effects. Instead the major oxidation-related issues are discussed and assessed for each system.

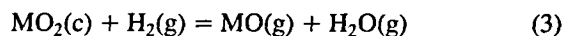
Vaporization

Another major degradation route is either simple vaporization or reaction to produce volatile products. Either may occur to the growing oxide scale on a nonoxide or to the surface of a structural oxide. The problem is to estimate the material loss rates from these processes and determine what temperatures yield maximum acceptable material loss rates.

Examples of reactions that produce volatile products are Simple vaporization:



Hydrogen reduction to a lower, volatile oxide:



Reaction with water vapor to produce a volatile hydroxyl species:



These processes are dependent on flow rates and total pressures. At low flow rates, high total pressures, or both, transport through the static boundary layer becomes important. At high flow rates and low pressures the situation approximates vaporization into a vacuum, and the flux leaving the surface is given by the Hertz-Knudsen-Langmuir equation (ref. 7):

$$J = \frac{\alpha_e P}{(2\pi MRT)^{1/2}} \quad (5)$$

Here J is a flux in mole per area-time, M is the molecular weight of the vapor, R is the gas constant, and T is the temperature. Note that this expression is modified by the evaporation coefficient α_e , which is defined as the actual flux leaving the surface divided by the maximum possible flux calculated from equation (5) with the equilibrium vapor pressure.

It is necessary to derive an expression that encompasses both of these effects. This was done by Bartlett (ref. 8) and is

modified here. The derivation is for simple vaporization (reaction (2)) into a flowing gas stream, but the general results apply to reactions (3) and (4) as well. The diffusive flux through the boundary layer is given by

$$J_D = h_m(P_{MO}^s - P_{MO}^\delta) \quad (6)$$

Here J_D is a diffusive flux in mole per area-time, h_m is the mass transfer coefficient, P_{MO}^s is the vapor pressure of MO(g) at the surface, and P_{MO}^δ is the vapor pressure of MO(g) at the outer edge of the boundary layer, which can be taken to be zero.

The vaporization reaction for the oxide MO(g) is given by



Assuming that both the forward and backward reactions are first order, the net flux J_v is given by

$$J_v = k_f[\text{MO(c)}] - k_b[\text{MO(g)}] \quad (8)$$

Here k_f is the forward rate constant, $[\text{MO(c)}]$ is the concentration of sites for vaporization from the solid, k_b is the backward rate constant, and $[\text{MO(g)}]$ is the concentration of MO(g). Reaction (8) can be simplified because $[\text{MO(c)}]$ is a constant, which can be incorporated into k_f , and $[\text{MO(g)}]$ is proportional to P_{MO}^s :

$$J_v = k_f - k_b P_{MO}^s \quad (9)$$

The reverse reaction or condensation rate is given by the number of molecules striking the surface, modified by α , the sticking coefficient. Thus the expression becomes

$$J_v = k_f - \frac{\alpha P_{MO}^s}{(2\pi MRT)^{1/2}} \quad (10)$$

Here M is the molecular weight of the vapor, R is the gas constant, and T is the absolute temperature. The forward rate constant can be expressed in terms of the equilibrium constant, because $K_{eq} = P_{MO}^{eq} = k_f/k_b$ and expression (10) becomes

$$J_v = \frac{\alpha P_{MO}^{eq}}{(2\pi MRT)^{1/2}} - \frac{\alpha P_{MO}^s}{(2\pi MRT)^{1/2}} \quad (11)$$

In a closed system J_v must go to zero and P_{MO}^s equals P_{MO}^{eq} , indicating that this expression is of the right form. The sticking coefficient α depends on a number of system parameters, such as pressure, temperature, and chemical composition. It is only known in a limited number of cases (ref. 7). Therefore calculations will be done for a range of α 's from 1 to 10^{-6} . Note also that the evaporation coefficient α_e in equation (5) is not

strictly the same as the sticking coefficient α (ref. 7). However, for the purposes of this calculation they will be taken as equal.

The vaporization flux must equal the diffusive flux described by equation (6). The unknown P_{MO}^s can be eliminated by equating these fluxes. Thus the expression for the flux of MO(g) is given by

$$J = \frac{\alpha P_{MO}^{eq} / (2\pi MRT)^{1/2}}{1 + \alpha / (2\pi MRT)^{1/2} h_m} \quad (12)$$

This is a general equation for vaporization into a flowing gas. Again it has the correct limits. For α close to 1, $\alpha / (2\pi MRT)^{1/2} h_m$ is much greater than 1, and the expression is similar to that for boundary layer transport alone (eq. (6)), indicating that the process is diffusion controlled. For α much less than 1, $\alpha / (2\pi MRT)^{1/2} h_m$ is also much less than 1, and the expression is similar to that for vaporization alone (eq. (5)), indicating that the process is reaction controlled. Also, when the velocity is very large, the mass transport coefficient becomes large, the boundary layer disappears, and equation (12) reduces to the expression for vaporization alone (eq. (5)).

Use of equation (12) allows an upper vapor pressure limit to be determined from an upper flux limit. The three types of refractory oxides dealt with in this report are silica, alumina, and zirconia. The results given herein are for silica vaporization. However, the results for the reactions that produce volatile species from alumina and zirconia are similar. For simplicity consider a hollow tube of diameter 4 ft (122 cm). First the mass transfer coefficient h_m must be calculated. By analogy with a similar heat transfer problem (ref. 9), h_m is given by

$$h_m = \frac{0.026 D_{MO}}{RTL} \left(\frac{\nu}{\rho D_{MO}} \right)^{0.33} \left(\frac{\rho \nu L}{\nu} \right)^{0.8} \quad (13)$$

Here D_{MO} is the diffusivity of MO in the gas, which for this situation is the diffusivity of SiO₂ vapor in 1 atm of combustion gas. From the Chapman-Enskog approximation D_{MO} is 2.5 cm²/sec at 1800 K (refs. 9 to 11). The term L is a characteristic sample dimension, taken as 122 cm; ν is the viscosity of air, taken as 6.1×10^{-4} g/cm-sec (ref. 12); ρ is the gas density, taken as a typical combustor velocity of 75 ft/sec (2.3×10^3 cm/sec); and ρ is the gas density, calculated to be 1.9×10^{-4} g/cm³ at 1 atm. Note that the last quantity in equation (13) is the Reynolds number, which has a value of 8.7×10^4 , indicating turbulent flow, as expected for a combustor.

Putting these values into equation (13) gives a value of 3.5×10^{-5} mol/cm²-sec for the mass transfer coefficient h_m at 1800 K and 1 atm. This gives the following expression for equation (12) for 1-atm total pressure:

$$J = \frac{0.1\alpha P_{M_0}^{eq}}{1 + 2860\alpha} \quad (14)$$

For 15 atm the diffusivity, the gas density, and the mass transfer coefficient change so that the expression becomes

$$J = \frac{0.1\alpha P_{M_0}^{eq}}{1 + 4762\alpha} \quad (15)$$

For 30 atm the diffusivity, the gas density, and the mass transfer coefficient change so that the expression becomes

$$J = \frac{0.1\alpha P_{M_0}^{eq}}{1 + 5556\alpha} \quad (16)$$

In order to calculate an upper limit of vapor pressure, a maximum allowable flux or material loss rate is necessary. There is no clear value for this. The calculations here will be done for two material loss rates; a rather liberal criterion of 10 mils/10 000 hr (0.025 $\mu\text{m/hr}$) and a more conservative criterion of 1 mil/10 000 hr (0.0025 $\mu\text{m/hr}$). The flux given here can be converted to a linear recession rate as follows:

$$R(\mu\text{m/hr}) = J(\text{mol/cm}^2\text{-sec}) \times M/\rho' \times 3.6 \times 10^7 \quad (17)$$

Here M is the molecular weight of the silica vapor and ρ' is the density of the solid oxide. For the refractory oxides discussed herein, M/ρ' is about 23.5 and equation (15) becomes

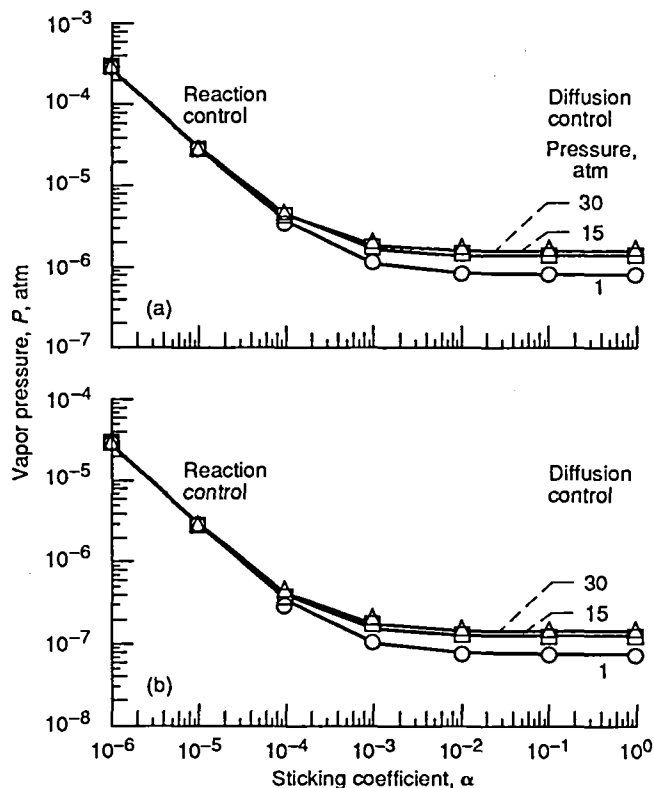
$$R(\mu\text{m/hr}) = 8.5 \times 10^8 \times J(\text{mol/cm}^2\text{-sec}) \quad (18)$$

For an acceptable rate of 0.025 $\mu\text{m/hr}$ a corresponding flux of 2.9×10^{-11} mol/cm²-sec is calculated; for an acceptable rate of 0.0025 $\mu\text{m/hr}$ a corresponding flux of 2.9×10^{-12} mol/cm²-sec is calculated.

The vapor pressures at 1, 15, and 30 atm, which give these fluxes, are shown in figures 5(a) and (b) as a function of α . These figures show the limits for equation (12) discussed earlier. For an $\alpha \geq 10^{-3}$, boundary layer transport is important. For an $\alpha < 10^{-4}$ the vaporization flux is described by the flux leaving the surface (eq. (5)). Qualitatively this means that if only a small fraction of the molecules that leave the surface can return and stick, the boundary layer offers no resistance. As a conservative estimate α can be taken as greater than 10^{-3} to get a maximum acceptable vapor pressure. Table I summarizes the vapor pressure limits for the two material loss rates at total pressures of 1, 15, and 30 atm. As figures 5(a) and (b) show, the limits for these pressures are close together. In the text the primary conditions for comparing the various materials will be 15 atm and 10 mils/10 000 hr.

TABLE I.—MAXIMUM ACCEPTABLE VAPOR PRESSURES

Pressure, atm	Material loss rate, mil/10 000 hr	
	10	1
	Maximum acceptable vapor pressure, atm	
1	8×10^{-7}	8×10^{-8}
15	10^{-6}	10^{-7}
30	10^{-6}	10^{-7}



(a) Material loss rate, 10 mils/10 000 hr.
(b) Material loss rate, 1 mil/10 000 hr.

Figure 5.—Vapor pressures as a function of sticking coefficient α .

It is important to recognize that the preceding calculation is only an approximation. The most obvious approximation would be that a fixed temperature was taken to estimate the terms in equation (12). This in turn was used to estimate a vapor pressure, and the vapor pressure will be used to determine a temperature. This is not strictly correct; an iterative approach should be used. However, the terms in equation (12) show only a fractional power dependence on temperature, and vapor pressure shows an exponential dependence on temperature. Therefore this approximation is reasonable.

The results in table I can be compared with previous calculations that were based on the Hertz-Knudsen-Langmuir expression (eq. (5)) and an evaporation coefficient of 1

(ref. 13). This approach gives the following relation of flux to pressure:

$$J = 0.1P \quad (19)$$

This relation gives acceptable vapor pressure limits of about 10^{-10} and 10^{-11} atm for 10 mils/10 000 hr and 1 mil/10 000 hr, respectively. Thus the consideration of diffusion through the boundary layer and a sticking coefficient of less than 1 has a strong effect on the calculations.

Having set an acceptable vapor pressure limit, the next step is to determine the vapor pressure for various materials as a function of temperature. This, in turn, can be used to set an upper use temperature. Note that upper temperatures calculated this way are only estimates—probably within ± 30 K. Specific cases of these calculations will be given in the following sections. Vapor pressures in these combustion atmospheres are calculated with a free-energy-minimization computer program, such as SOLGASMIX-PV (ref. 14) or NASA CEC (ref. 3). This type of program takes the composition of the material in question and the gas atmosphere and determines the equilibrium quantities of the condensed and gaseous species. The best thermodynamic data available were used for these calculations. Most of the data were taken from the JANAF tables (ref. 15) and from the compendium of Barin and Knacke (refs. 16 and 17), when not available from JANAF. Whenever possible, checks were made by using both free-energy-minimization programs.

Interfacial Reactions

Interfacial reactions are not directly a result of environmental interactions. An example of an important interfacial reaction is the reaction of an oxide scale and a nonoxide substrate. Such a reaction may generate large gas pressures and damage the protective oxide scale. It may also consume the oxide scale. Another deleterious reaction can occur at the fiber/matrix interface. Ceramic-matrix composites obtain their desirable mechanical properties from a loosely bonded interface. An interaction that generates gas pressures at this interface, that leads to fiber/matrix bonding, or both can destroy the desirable interfacial properties.

In the next section these degradation routes will be discussed for each candidate material in the fuel-lean and fuel-rich environments. Because interfacial reactions are similar in both environments, a separate section is devoted to interfacial reactions.

Specific chemical processes leading to degradation are identified and their relative importance assessed. Where possible, maximum use temperatures are predicted.

Durability of Candidate Nonoxide Ceramics

Fuel-Lean Environment

The candidate nonoxide ceramics include SiC, Si_3N_4 , MoSi_2 , and AlN. First, consider the silicon-base ceramics, which generally show good durability in this environment owing to the formation of a protective silica scale. Silica is the least permeable oxide to oxygen (ref. 2), but it can still grow rapidly at high temperatures. Silicon-base ceramics oxidize according to the following reactions:

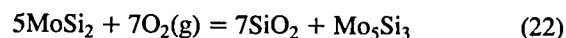
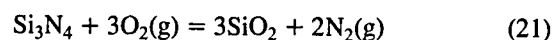
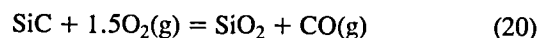


Figure 6 shows some high-temperature isothermal oxidation rates for silicon-base ceramics (refs. 18 to 22). The growth rates indicate good behavior under isothermal conditions in pure oxygen. However, care must be taken in extrapolating this information to real combustion environments, which include thermal cycling and water vapor effects.

Information on cyclic oxidation of silicon-base ceramics is limited (refs. 23 to 25). The various phase changes of silica would be expected to have a major effect on the cyclic oxidation of silicon-base ceramics. The equilibrium diagram shows the following transformations (ref. 26):

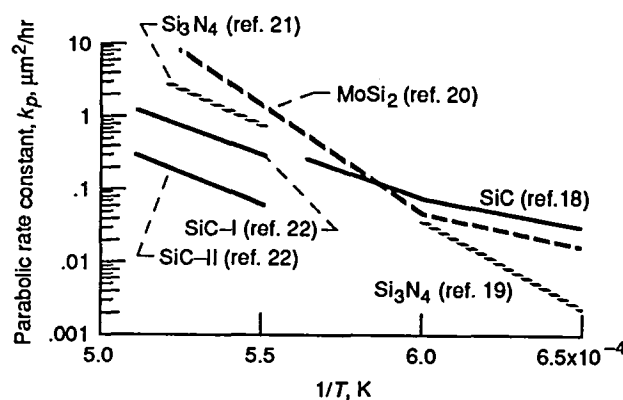


Figure 6.—Parabolic oxidation rates for SiC, Si_3N_4 , and MoSi_2 .

846 K 1143 K 1743 K 1986 K
 α -quartz = β -quartz = β_2 -tridymite = β -cristobalite = Liquid
 (23)

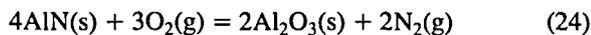
The commonly observed oxidation phases are quartz and cristobalite. Although the phase transformations are sluggish, the resultant structural changes may lead to enhanced oxidation. One mechanism for this is simple cracking of the scale due to the phase changes. Another mechanism for enhanced oxidation on cycling may be oxide cracking due to the different coefficients of thermal expansion of silica and the ceramic substrate. Even a small change in the oxidation rate could be significant over the 18 000-hr lifetime projected for the HSCT combustor liner.

This issue of phase transformations in the protective scale includes the melting point limitation (1986 K). Silicon-base ceramics are somewhat unique in that the scale melts at a lower temperature than the substrate melts. Above the melting point the scale could easily be blown off in the flowing gases of the combustor, and rapid transport rates through a liquid scale would very likely lead to limited protection and unacceptably high growth rates. Even before the melting point of silica is reached, the scale may tend to soften and lead to more rapid transport rates. Small amounts of metal ion impurities may tend to exacerbate this situation.

Figure 2 shows that combustion atmospheres contain up to 10% water vapor. It is well known that the oxidation of silicon is accelerated in steam atmospheres (ref. 27). Water is also known to accelerate the oxidation of SiC and Si₃N₄ (refs. 28 and 29) by an order of magnitude or so. This may occur by inducing phase transformations that lead to scale cracking by creating conditions for more rapid diffusion rates through the scale (ref. 30).

Recent experiments at the Lewis Research Center have shown that after a brief increase in oxidation temperature of about 150 deg K and then a return to the original temperature, reaction rates for Si₃N₄ increase by about an order of magnitude (ref. 31). Clearly this observation has some significant implications for the application of silicon-base ceramics in combustion environments, where such thermal excursions are common.

Aluminum nitride forms a protective oxide according to



The alumina scale has been observed to be dense and protective to about 1773 K in dry oxygen. However, at 1873 K the alumina scale was observed to be porous owing to N₂(g) escape (ref. 32). Figure 7 shows the accelerated oxidation of AlN in the presence of water vapor (ref. 33). In contrast to the silicon-base ceramics there is only limited information on the oxidation of AlN at high temperatures.

Once a stable protective oxide film has formed on a nonoxide, the next issue to consider is the vaporization of that film. The vaporization of Al₂O₃ on AlN is discussed in the

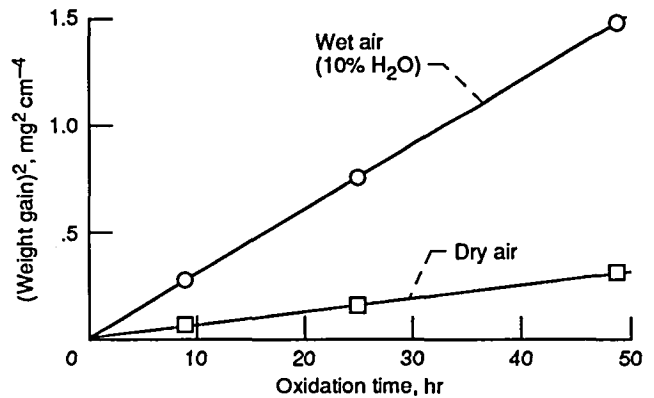


Figure 7.—Oxidation kinetics of AlN in dry and wet air. Temperature, 1523 K. From reference 33.

next section; SiO₂ vaporization is discussed here. SiO₂ vaporizes according to these reactions:



Figure 8 shows the vapor pressures of species above SiO₂ in the fuel-lean environment. Table II lists the maximum use temperatures for silica due to material loss from volatility. Taking standard conditions as a pressure of 15 atm and an acceptable loss rate of 10 mils/10 000 hr, one arrives at a maximum use temperature of 2060 K.

Related to this are some observations on the volatilization of silica in steam. Cheng and Cutler (ref. 34) have observed that silica coupons rapidly lose weight in 0.84 atm of steam. They observed the maximum weight losses at 1573 K and attributed these effects to production of Si(OH)₄:



In a combustion environment there is about 10% water vapor. However, recent unpublished experiments at the Lewis

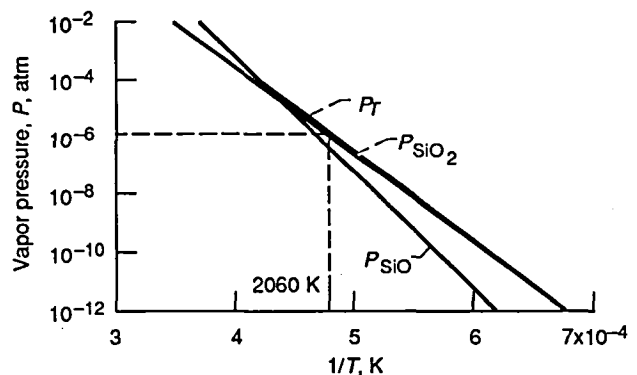


Figure 8.—Vapor pressure of species above SiO₂ in fuel-lean environment.

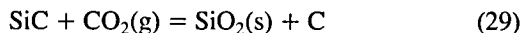
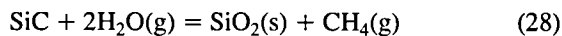
TABLE II.—MAXIMUM USE TEMPERATURES FOR OXIDES BASED ON VOLATILITY— 15 atm TOTAL PRESSURE

Material	Fuel lean	Fuel rich
	Maximum use temperature, K	
Material loss rate, 10 mils/10 000 hr		
SiO ₂	2060	1770
Al ₂ O ₃	2170	2150
Mullite	2080	1800
TiAl ₂ O ₅	2130	2130
Y ₂ O ₃ · 2(ZrO ₂)	2600	2560
Material loss rate, 1 mil/10 000 hr		
SiO ₂	1940	1640
Al ₂ O ₃	2000	1980
Mullite	1940	1690
TiAl ₂ O ₅	1980	1960
Y ₂ O ₃ · 2(ZrO ₂)	2440	2410

Research Center by K.N. Lee and N.S. Jacobson on a silica coupon at 1573 K in 10% water vapor/oxygen streams have shown no evidence of volatility due to this reaction.

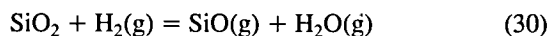
Fuel-Rich Environments

Figure 2 shows the predicted temperatures and gas environments for this region. Temperatures are slightly higher than in the fuel-lean region, and the gas environments contain large amounts of H₂ and CO. However, the gas environments also contain H₂O and CO₂, which are oxidants. For this reason active oxidation is unlikely and SiO₂ would be expected to form on silicon-base ceramics. Stability diagrams (fig. 9) for a range of carbon activities in the Si-C-N-H-O system at 1773 K show SiO₂ to be the stable phase in the fuel-rich environment. Diagrams at lower temperatures give the same result. Examples of possible oxidation reactions are

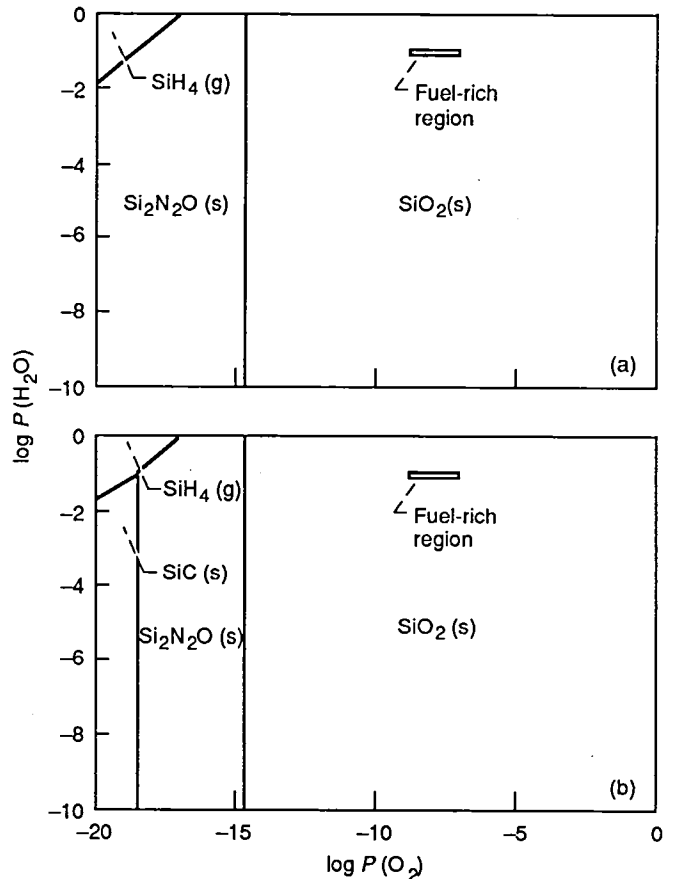


The basic questions with the fuel-rich environment deal with the stability of this silica scale. Because it will be grown with H₂O and CO₂ as the primary oxidants, the question is, Will it be as protective and dense as a scale grown in a dry oxygen environment? Related to this is the possibility of more rapid scale growth rates in these environments.

A major issue is how hydrogen affects the reduction of the silica scale according to



The presence of water vapor in the environment will suppress this reaction to some degree. However, enough SiO(g) is



(a) $a(\text{C}) = 10^{-4}$.
(b) $a(\text{C}) = 1$.

Figure 9.—Stability diagrams for Si-C-N-O-H with $P(\text{N}_2) = 0.69$ atm at 1773 K.

produced to give much higher total vapor pressures than in the fuel-lean situation. The vapor pressures in the fuel-lean and fuel-rich environments can be compared by examining figures 8 and 10. Table II lists the maximum use temperature in the fuel-rich environment. For the primary criteria of 15 atm and 10 mils/10 000 hr this limit is 1770 K—substantially less than the fuel-lean limit of 2060 K.

In the fuel-rich environment an oxide film would very likely form by reaction (28) or (29) and then vaporize by reaction (30). This is a situation of parabolic kinetics where the net recession rate is described by both the parabolic rate constant for oxidation and the linear rate constant for volatilization. This situation has been described by Tedmon (ref. 35) and the net recession rate is given by

$$\frac{dy}{dt} = \frac{k_{p,r}}{2y} + k_{l,r} \quad (31)$$

Here dy/dt is the recession rate, y is the net recession, $k_{p,r}$ is the parabolic recession rate due to oxidation, $k_{l,r}$ is the linear recession rate due to volatility. Depending on

Inserted
3-19-92
mpp

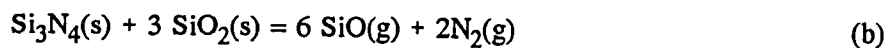
ERRATA

NASA Technical Paper 3162 HIGH-TEMPERATURE DURABILITY CONSIDERATIONS FOR HSCT COMBUSTOR

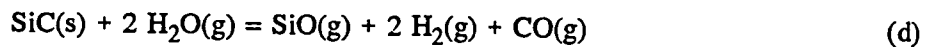
Nathan S. Jacobson

Add to p. 8, Durability of Nonoxide Ceramics, Fuel-Rich Environments, paragraph 1.

Following Wagner (ref. A), the critical equilibria for a stable SiO₂ scale formation are (ref. B)



Sufficient SiO must be formed to maintain these equilibria. The SiO can form from any oxidant (e.g., CO₂ or H₂O; ref. C):



Thus, in the fuel-rich environment, active oxidation is not expected.

References

- A. Wagner, C.: Passivity During the Oxidation of Silicon at Elevated Temperatures. J. Appl. Phys., vol. 29, no. 9, 1958, pp. 1295-1297.
- B. Singhal, S.C.: Thermodynamic Analysis of the High-Temperature Stability of Silicon Nitride and Silicon Carbide. Ceramurgia Int., vol. 2, no. 3, 1976, pp. 123-130.
- C. Heuer, A.H.; and Lou, V.L.K.: Volatility Diagrams for Silica, Silicon Nitride, and Silicon Carbide and Their Application to High-Temperature Decomposition and Oxidation. J. Am. Ceram. Soc., vol. 73, no. 10, 1990, pp. 2789-2803.

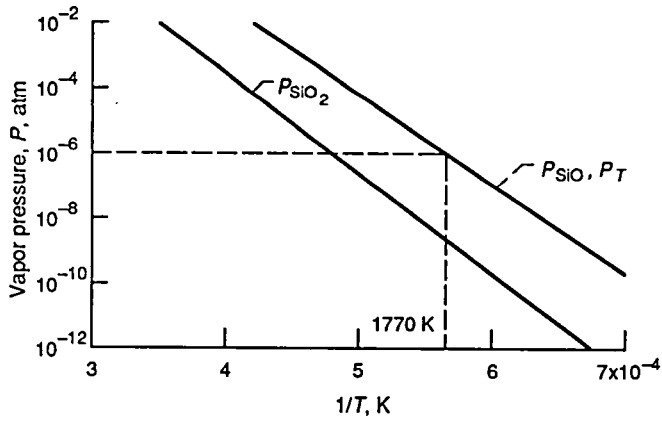
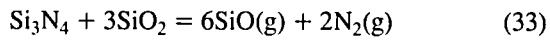
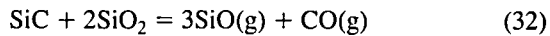


Figure 10.—Vapor pressure of species above SiO_2 in fuel-rich environment.

their relative rates, these may combine to reduce the maximum use temperature to below 1770 K.

Interfacial Reactions

As mentioned, interfacial reactions are similar in both the fuel-lean and fuel-rich environments. An important reaction is that of the protective silica layer with the carbide or nitride substrate according to the following reactions:



These reactions have been stated to be intrinsic limitations of SiC and Si_3N_4 (in an unpublished Wright Patterson program review by W.L. Worrell). The issue is that the reactions of the two solids create substantial gas pressures at the SiC/SiO₂ interface at high temperatures. Figure 11 shows a plot of total pressure versus temperature for these reactions. When the total pressure equals the ambient, the scale may become unstable and be ruptured. Figure 11 indicates that the total pressure equals 1 atm above 2000 K for stoichiometric SiC and Si_3N_4 and silicon-rich SiC and Si_3N_4 . Because this is above the melting point for SiO_2 , the melting point will be an issue before the high gas pressures are reached. However, many types of SiC contain excess carbon. In these cases the carbon activity in SiC is unity. Figure 11 also shows the total pressure generated from reaction (32) for carbon-rich SiC. Note that higher gas pressures are generated at lower temperatures than for stoichiometric SiC. Furthermore SiO_2 is not stable above 1750 K in the presence of carbon-rich SiC. Thus the reaction of SiO_2 with the substrate is primarily an issue with carbon-saturated SiC. Recent experimental work at the Lewis Research Center has shown that this is a complex reaction with several steps (ref. 36).

Another important interfacial reaction is the interaction of the fiber with the matrix. Such reactions have been discussed by other investigators (ref. 37) and are only briefly discussed herein. Ceramic-matrix composites rely on a loosely bonded

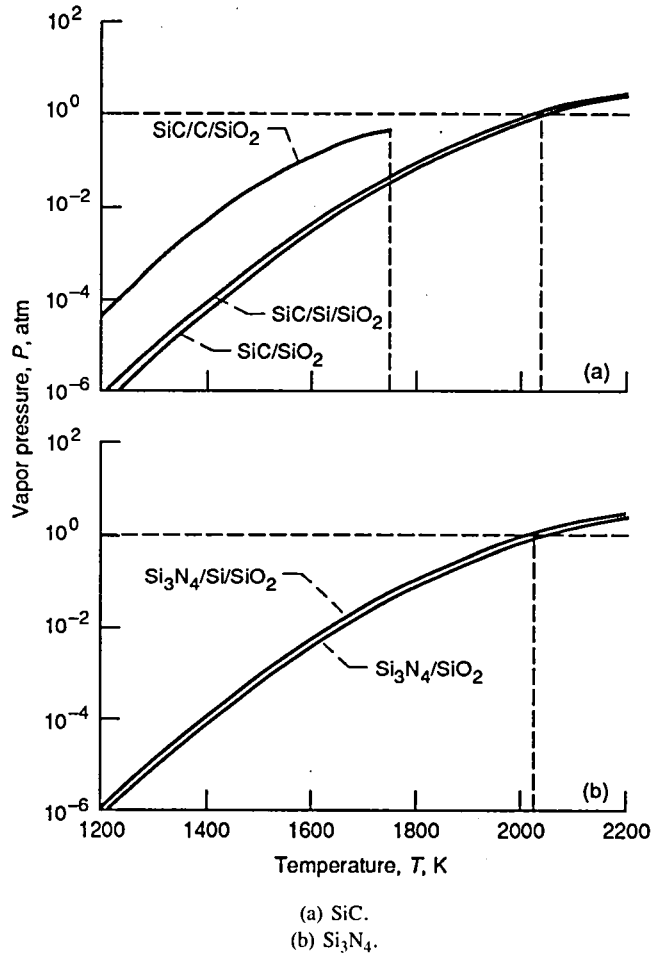
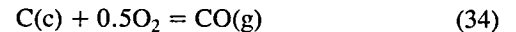
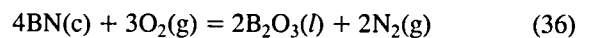


Figure 11.—Total pressure from interfacial reactions of SiO_2 as a function of temperature.

fiber in a matrix for good fracture properties. Various fiber coatings have been applied to achieve this. The most common coatings include carbon and boron nitride. The immediate concern with these coatings is attack by oxygen penetrating the matrix. Carbon will oxidize as



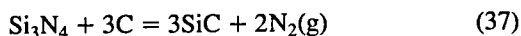
Such reactions will generate large gas pressures at the fiber/matrix interface, possibly damaging the composite. In addition, the loosely bound interface will be destroyed, leading to a degradation in properties. Boron nitride will oxidize as



This oxidation reaction generates gas pressures at the fiber/matrix interface that may damage the composite. In addition, the liquid B_2O_3 product may destroy properties of the fiber/matrix interface. It is not possible to put a maximum use

temperature on these degradation routes; rather they are consequences to be aware of in the event of a crack.

A composite system that looks promising is a carbon-coated SiC fiber in an Si₃N₄ matrix. However, the carbon is predicted to react directly with the matrix:



At temperatures above 1683 K the pressure of nitrogen generated exceeds 1 atm (ref. 37). These issues with carbon and boron nitride indicate the need for a more durable fiber coating.

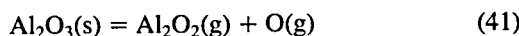
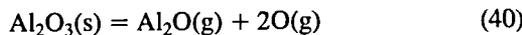
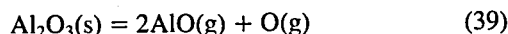
Related to these interfacial coatings is the inherent stability of the fiber. The most common nonoxide fiber is SiC. However, some of these fibers contain various impurities. Reactions such as (32) clearly indicate that SiO₂ and C impurities can lead to low-temperature fiber degradation (ref. 38). A fiber with a composition close to that of pure SiC is most desirable.

Durability of Candidate Oxide Ceramics

Fuel-Lean Environments

Four materials are discussed here—pure alumina (Al₂O₃); mullite [3(Al₂O₃) · 2(SiO₂)]; titanium aluminate [(TiO₂) · (Al₂O₃)]; yttrium-aluminum-garnet [3(Y₂O₃) · 5(Al₂O₃)], or YAG; and yttria fully stabilized zirconia [Y₂O₃ · 2(ZrO₂)]. The advantage of these materials is that oxidation-related issues are not problems. The major chemical limitations are volatility and the phase changes. Note that the discussion of Al₂O₃ vaporization is applicable to the oxidized AlN ceramic.

First consider the alumina-base oxides. Alumina is known to undergo a complex vaporization scheme (ref. 39):



These reactions have been studied in a Knudsen cell under a vacuum. For this reason there is some question about reaction (42). Nonetheless recent work has shown that this reaction is expected to proceed in the presence of oxygen (ref. 40). The other reactions would be suppressed in the presence of oxygen. By using the thermodynamic data obtained from Knudsen cell measurements, the expected partial pressures of each species in an oxidizing atmosphere can be calculated.

Thermodynamic predictions also indicate that the alumina hydroxyl species (ref. 15) is readily produced in the presence of water vapor at high temperatures according to



The species AlOH(g) is also predicted to form in smaller amounts. Because it is difficult to study these species at very high temperatures in oxidizing environments, there is limited experimental information on them. Figure 12 shows the vapor pressure of Al₂O₃ in the fuel-lean environment. Clearly the dominant species is AlO₂H(g). The maximum use temperatures for pure Al₂O₃ are shown in table II. The primary criteria of 15 atm and 10 mils/10 000 hr give a maximum use temperature of 2170 K. If AlO₂H(g) is not formed, the maximum use temperature is substantially higher.

The double oxides containing alumina (i.e., mullite, YAG, and aluminum titanate) appear to show similar behavior. The data for mullite are shown in figure 13. The silica in solution has a high vapor pressure that is comparable to that of AlO₂H(g). Solid-solution vapor pressure lowering does not appear to give much benefit over pure silica. YAG would be expected to show somewhat lower vaporization behavior

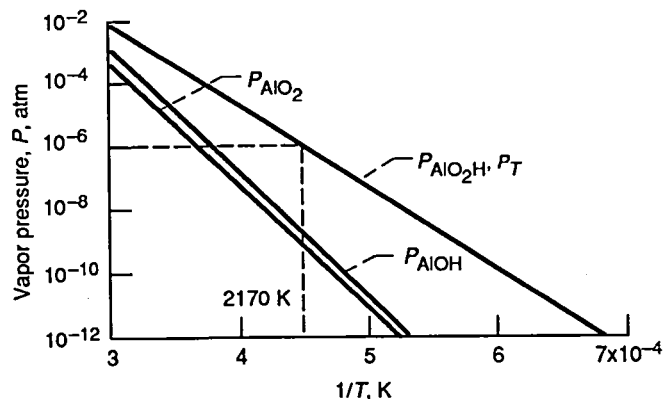


Figure 12.—Vapor pressure of principal species above Al₂O₃ in fuel-lean environment.

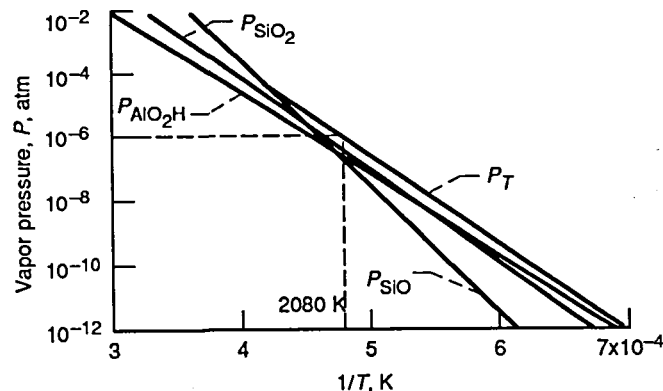


Figure 13.—Vapor pressure of principal species above mullite in fuel-lean environment.

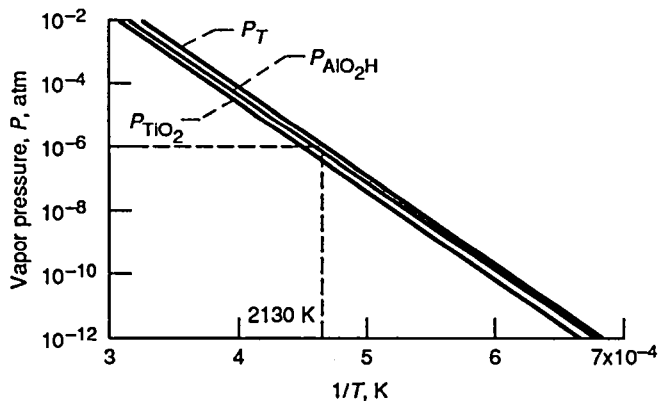


Figure 14.—Vapor pressure of principal species above TiAl_2O_5 in fuel-lean environment.

TABLE III.—MELTING POINTS OF REFRACTORY OXIDES

Oxide	Melting point, K
SiO_2	1996
Al_2O_3	2327
Mullite	2063
$3(\text{Y}_2\text{O}_3) \cdot 5(\text{Al}_2\text{O}_3)$	~2173
TiOAl_2O_3	~2123
$\text{Y}_2\text{O}_3 \cdot 2(\text{ZrO}_2)$	~2973
$\text{Yb}_2\text{O}_3 \cdot 3(\text{ZrO}_2)$	~3100
$\text{Dy}_2\text{O}_3 \cdot 5.7(\text{ZrO}_2)$	~3020
$\text{Ho}_2\text{O}_3 \cdot 4(\text{ZrO}_2)$	~3030
$\text{Er}_2\text{O}_3 \cdot 4(\text{ZrO}_2)$	~3060

because of the low volatility of Y_2O_3 (ref. 41). Unfortunately there are no solid-solution data available on YAG. The alumina-saturated composition would behave like pure alumina; the yttria-saturated composition may have vapor pressures substantially lower than those of pure alumina. As shown in figure 14, TiAl_2O_5 has a low vapor pressure. However, it decomposes to TiO_2 and Al_2O_3 at temperatures between 1173 and 1523 K (ref. 42)—clearly a major issue. The maximum use temperatures for these oxides are shown in table II.

Another issue to consider with alumina-base ceramics is the melting point. Table III lists the melting points for various refractory oxides (ref. 43). In general, these are high enough that they are not directly at the temperatures of concern for the HSCT combustor.

Next consider the zirconia-base oxides, which are among the most chemically stable ceramics at high temperatures. On heating, pure zirconia undergoes a destructive monoclinic-to-tetragonal phase change at about 1223 K. The solution to this problem has been to add a second oxide. A small amount of second oxide stabilizes a mixture of tetragonal and monoclinic phases to about 1900 K and is termed "partially stabilized

zirconia." A larger amount of second oxide stabilizes the cubic phase to much higher temperatures. For this reason the focus of this section is on fully stabilized zirconia. The stability of yttria fully stabilized zirconia is shown in the phase diagram in figure 15 (ref. 44).

The thermodynamic properties of a number of metal oxide-zirconia systems have recently been reviewed (ref. 41). Zirconia has been fully stabilized by both alkaline earth oxides and rare earth oxides. The alkaline earth oxide stabilizers tend to vaporize preferentially at low temperatures and thus are not really suitable for high-temperature structural materials. Rare-earth-stabilized zirconias show much more promise. In particular the systems $\text{Y}_2\text{O}_3\text{-ZrO}_2$, $\text{Yb}_2\text{O}_3\text{-ZrO}_2$, $\text{Dy}_2\text{O}_3\text{-ZrO}_2$, $\text{Ho}_2\text{O}_3\text{-ZrO}_2$, and $\text{Er}_2\text{O}_3\text{-ZrO}_2$ look promising. These have very low vapor pressures and large cubic phase fields stable to very high temperatures. The latter four compounds are especially interesting because they exhibit liquidus maxima in the phase diagram, suggesting strong solid-solution interactions and even lower volatility. The high melting point of each compound is listed in table III.

Solid-solution data were only available for yttria fully stabilized zirconia [$\text{Y}_2\text{O}_3 \cdot 2(\text{ZrO}_2)$]. The vapor pressure of this material in the fuel-lean environment is shown in figure 16. Table II gives the maximum use temperatures for this material. The primary criteria of 15 atm and 10 mils/10 000 hr give a maximum use temperature of 2600 K—the highest of any of the materials discussed.

Water vapor interactions are also a potential issue for zirconia-base ceramics. Some rare earth stabilizers may be

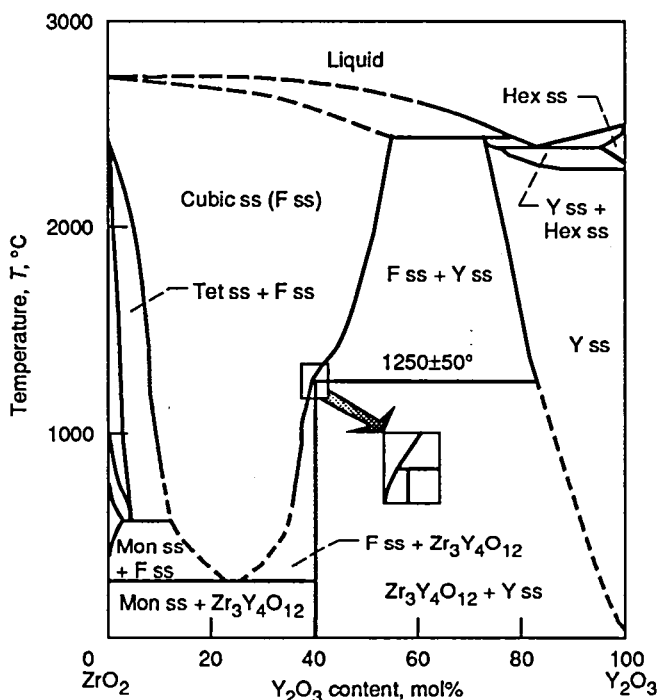


Figure 15.—Phase diagram for system $\text{Y}_2\text{O}_3\text{-ZrO}_2$, where F = fluorite type of ZrO_2 ; Y = Y_2O_3 ; Tet = tetragonal; Mon = monoclinic; Hex = hexagonal; and ss = solid solution. From reference 44.

hygroscopic. There is some evidence that water may induce deleterious phase changes in stabilized zirconias (ref. 45).

Fuel-Rich Environments

Structural alumina has been predicted to hold up well in a hydrogen environment (ref. 46). Therefore the alumina-base materials are expected to perform well in fuel-rich environments. The calculations verify this, as shown in figures 17 to 19. Table II lists the calculated maximum use temperatures. The primary criteria of 15 atm and 10 mils/10 000 hr give a maximum use temperature of 2105 K for alumina. Note that mullite has substantially lower volatility limits than the other alumina- and zirconia-base oxides. The reduction of SiO_2 (in mullite) creates large pressures of $\text{SiO}(\text{g})$, leading to these lower limits. TiAl_2O_5 has slightly lower limits than Al_2O_3 because of the contribution of $\text{TiO}_2(\text{g})$. Surprisingly $\text{TiO}(\text{g})$ is not predicted to form in appreciable quantities.

Zirconia-base materials have also been predicted to show good behavior in a hydrogen environment. Therefore $\text{Y}_2\text{O}_3 \cdot 2(\text{ZrO}_2)$ would be expected to be quite stable in fuel-rich environments. Calculations support this, as shown in figure 20. Note that $\text{ZrO}(\text{g})$ and $\text{YO}(\text{g})$ do not form in any appreciable quantities. Table II lists the maximum use temperature for this material. The primary criteria for $\text{Y}_2\text{O}_3 \cdot 2(\text{ZrO}_2)$ give a limit of 2560 K in fuel-rich environments.

Interfacial Reactions

As mentioned, fiber-reinforced, oxide-matrix composites are under development for engine applications. As in the case of silicon-base ceramic-matrix composites (CMC's), a loosely bound interface is critical. In general, fiber-reinforced, oxide-matrix composites are not as well developed as fiber-reinforced, silicon-base ceramics. It is beyond the scope of this report to discuss the various types of oxide-base CMC's. Some proposed oxide-base CMC's involve a nonoxide fiber (e.g., SiC or TiB_2). In these cases matrix cracking and subsequent fiber oxidation are issues. Also matrix reduction

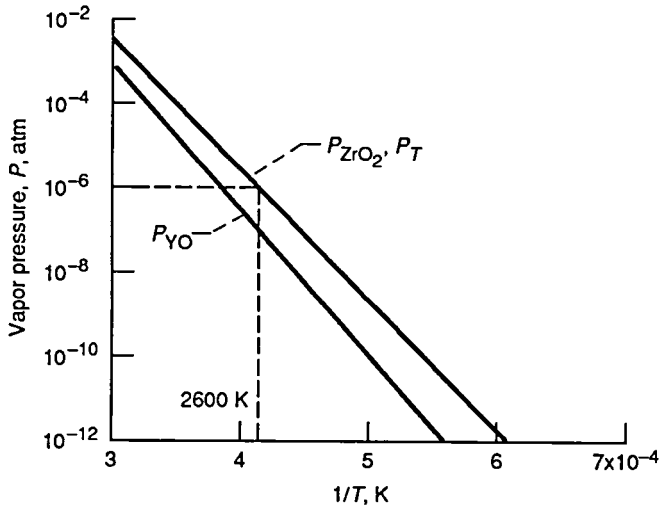


Figure 16.—Vapor pressures of principal species above $(\text{Y}_2\text{O}_3) \cdot 2(\text{ZrO}_2)$ in fuel-lean environment.

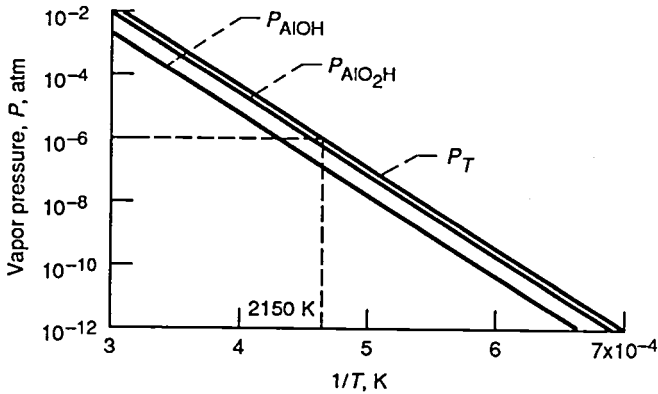


Figure 17.—Vapor pressure of principal species above Al_2O_3 in fuel-rich environment.

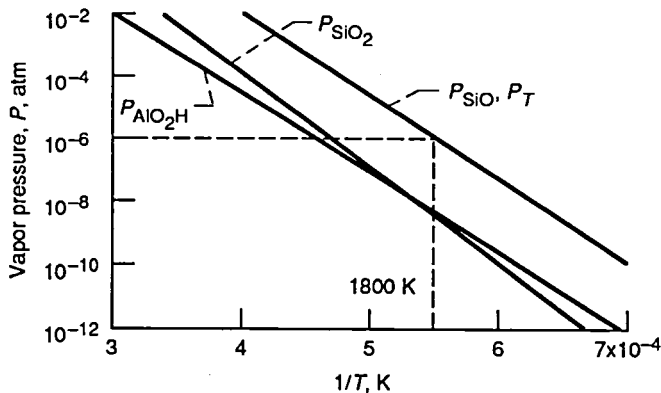


Figure 18.—Vapor pressures of principal species above mullite in fuel-rich environment.

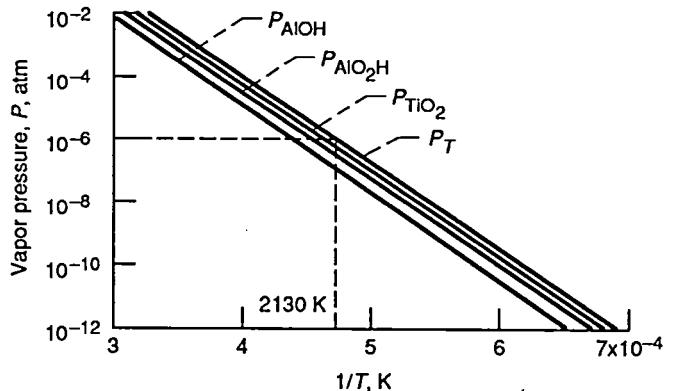


Figure 19.—Vapor pressure of principal species above TiAl_2O_5 in fuel-rich environment.

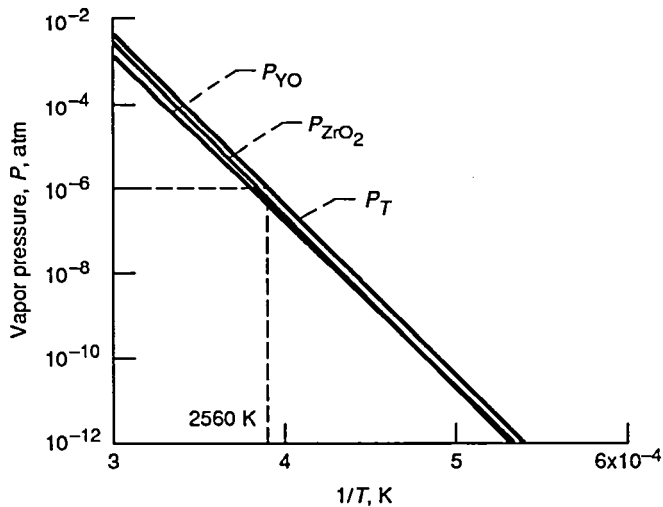


Figure 20.—Vapor pressure of principal species above $(Y_2O_3) \cdot 2(ZrO_2)$ in fuel-rich environment.

by the fiber is an issue. Other oxide-base CMC's involve an oxide fiber in an oxide matrix. In these cases fiber/matrix interactions can be assessed from oxide phase diagrams. Alumina-fiber-reinforced alumina is perhaps the most developed of these. Interactions have been prevented by a ZrO_2 or SnO_2 fiber coating (refs. 47 and 48).

Summary of Results and Conclusions

The goals of this report have been threefold: (1) to define the High Speed Civil Transport (HSCT) combustor environment, (2) to identify the major routes for candidate ceramic degradation, and (3) to determine the relative importance of these routes and, where possible, calculate a maximum use temperature for each candidate ceramic.

The emphasis of the report has been on the rich burn/quick quench/lean burn (RQL) and lean premixed/prevaporized (LPP) combustor designs. The lean-burn regions of both combustors consist primarily of N_2 , O_2 , CO_2 , and H_2O . The rich-burn region of the RQL combustor consists primarily of N_2 , CO , H_2 , CO_2 , and H_2O . Temperatures may be as high as 2000 K, pressures are projected to be about 15 atm, and flow velocities are about 50 to 100 ft/sec (15.24 to 30.48 m/sec).

Three major routes of degradation for candidate liner materials in these environments have been identified. These routes are (1) oxidation, (2) vaporization, and (3) interfacial reactions. The first is difficult to quantify because factors such as cycling and water vapor are expected to have a major effect. There are not enough experimental data on these factors to incorporate them into a model. Vaporization effects have been considered by modeling the combustor as a hollow cylinder with the walls vaporizing through a boundary layer into a flowing gas. This allows a maximum acceptable vapor pressure, and hence temperature, to be determined. Interfacial reactions can be predicted and noted when they are likely to be a problem.

The major degradation route for the nonoxide ceramics (SiC , Si_3N_4 , $MoSi_2$, and AlN) in fuel-lean environments is expected to be oxidation. This will likely be enhanced by water vapor and cycling effects. In fuel-rich environments $SiO(g)$ formation from $H_2(g)$ reduction of the $SiO_2(s)$ scale is likely to be an issue. For the oxide ceramics (alumina- and zirconia-base oxides) volatility is a key issue.

As mentioned in the introduction, materials selection is often a tradeoff between chemical, mechanical, and physical properties. The high thermal conductivity and desirable mechanical properties of the nonoxide ceramics make them the leading candidates for the HSCT program. However, oxide ceramics clearly offer better environmental resistance. One option is an oxide-coated, silicon-base ceramic, which is described in the appendix. Ultimately oxides are the most durable at the highest temperatures.

Acknowledgment

Thanks are due to Carl Stearns of Sverdrup Technology Inc., Lewis Research Center Group, for providing the burner flame temperatures as a function of equivalence ratio. Helpful discussions with S. Gokoglu and J. Doychak of NASA Lewis and J.T. Porter II of MSNW, San Marcos, California, are very much appreciated.

Lewis Research Center
National Aeronautics and Space Administration
Cleveland, Ohio, August 12, 1991

Appendix—Oxide Coatings on SiC

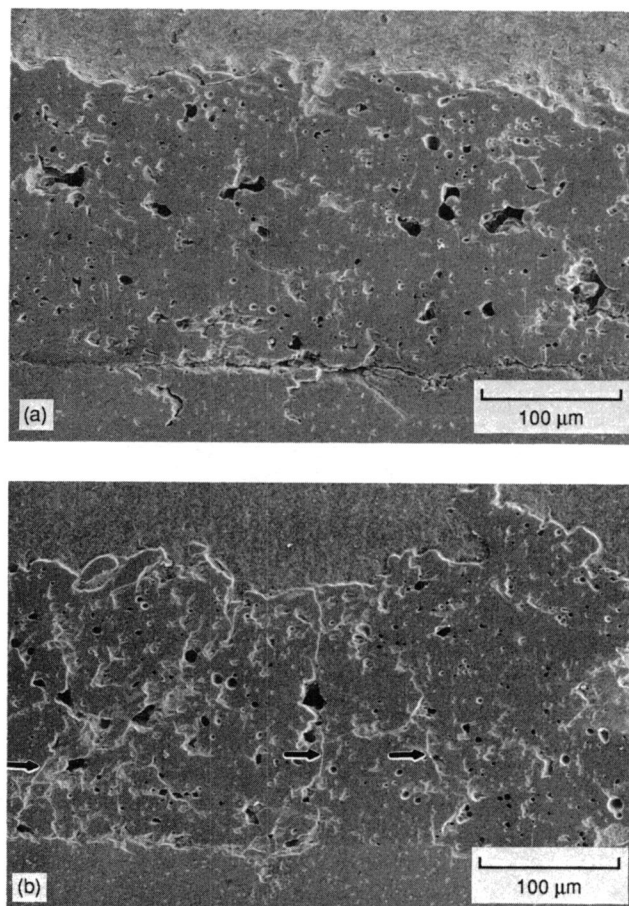
For application in the HSCT combustor, silicon-base ceramics show the most desirable physical and mechanical properties. However, the oxide ceramics show the best environmental resistance. An optimum system therefore might be a refractory-oxide-coated, silicon-base ceramic. This would differ from a more conventional thermal-barrier-coated metal, where the ceramic coating is porous. In this case a dense coating to block the transport of oxygen, water vapor, and hydrogen to the silicon ceramic is required. Thus a close match of thermal expansions is necessary. A list of coefficients of thermal expansions (refs. 26 and 49) for these materials is given in table IV. Note that mullite has a coefficient of thermal expansion close to that of SiC.

Solar Turbines, Inc., of San Diego has done extensive work on coating SiC tubes with refractory oxides for corrosion resistance (ref. 50). As expected, they have found that mullite holds up the best. A cross section of such a coating is shown in figure 21(a). The difficulty with these coatings is that on thermal cycling they tend to crack, as shown in figure 21(b). It is not clear if these cracks are due to the slight mismatch in thermal expansion or to residual stresses that developed in the coating process. Heating the substrate during coating appeared to help but did not eliminate the problem. Clearly more work is needed in this area.

Even if a durable mullite coating could be formed, it would only provide protection against some degradation routes. It

TABLE IV.—COMPARATIVE
THERMAL EXPANSION
COEFFICIENTS AT 1300 K

Material	Comparative thermal expansion coefficient, K^{-1}
Si_3N_4	3.7×10^6
SiC	5.8
Mullite	5.3
Al_2O_3	9.9
$TiAl_2O_5$	9.5
ZrO_2	10.5



(a) As-received coating.
(b) After two 24-hr cycles at 1273 K.

Figure 21.—Plasma-sprayed mullite coating on SiC with boron and carbon sintering additives.

should provide oxidation protection by limiting access of oxygen and water vapor to the silicon ceramic and also by reducing the temperature of the silicon ceramic surface. It will not provide resistance to hydrogen reduction of SiO_2 to $SiO(g)$; as discussed in the report, the SiO_2 in the mullite is reduced by hydrogen. It may be possible to prevent this degradation route by making a graded coating to alumina.

References

- Ott, J.: Researchers Seek Technologies for Quiet, Environmentally Safe SST. *Av. Week Space Technol.*, vol. 132, no. 25, June 18, 1990, pp. 94-95, 98.
- Shaw, N.J., et al.: Materials for Engine Applications Above 3000 °F—An Overview. NASA TM-100169, 1987.
- Gordon, S.; and McBride, B.J.: Computer Program for Calculation of Complex Chemical Equilibrium Compositions, Rocket Performance, Incident and Reflected Shocks, and Chapman-Jouguet Detonations. NASA SP-273, 1971.
- Glassman, I.: *Combustion*. Academic Press, 1977.
- Jacobson, N.S.: Sodium Sulfate: Deposition and Dissolution of Silica. *Oxid. Met.*, vol. 31, no. 1/2, 1989, pp. 91-103.
- Jacobson, N.S.; Smialek, J.L.; and Fox, D.S.: Molten Salt Corrosion of SiC and Si₃N₄. *Handbook of Ceramics and Composites, Vol. I: Synthesis and Properties*, N.P. Cheremisinoff, ed., Marcel-Dekker, 1990, pp. 99-135.
- Searcy, A.W.: The Kinetics of Evaporation and Condensation Reactions. *Chemical and Mechanical Behavior of Inorganic Materials*, A.W. Searcy, D.V. Ragone, and U. Colombo, eds., Wiley-Interscience, 1970, pp. 107-133.
- Bartlett, R.W.: Platinum Oxidation Kinetics With Convective Diffusion and Surface Reactions. *J. Electrochem. Soc.*, vol. 11, no. 6, 1967, pp. 547-550.
- Geiger, G.H.; and Poirier, D.R.: *Transport Phenomena in Metallurgy*, Addison-Wesley, 1974, p. 244.
- Bird, R.B.; Stewart, W.E.; and Lightfoot, E.N.: *Transport Phenomena*, Wiley, 1960.
- Svehla, R.A.: Estimated Viscosities and Thermal Conductivities of Gases at High Temperatures. NASA TR R-132, 1961.
- Weast, R.C.; and Astle, M.J.: eds.: *Handbook of Chemistry and Physics*, 60th ed., CRC Press, Boca Raton, FL, 1980.
- Jacobson, N.S.: Environmental Durability Issues for Ceramic Materials. *HITEMP Review 1990*, NASA CP-10051, 1990, pp. 62-1 to 62-9.
- Besmann, T.M.: SOLGASMIX-PV: A Computer Program to Calculate Equilibrium Relationships in Complex Chemical Systems. ORNL/TM-5775, Oak Ridge National Laboratory, Apr. 1977.
- Chase, M.W., Jr., et al., eds.: *JANAF Thermochemical Tables*, 3rd ed., American Chemical Society and American Physical Society, New York, NY, 1985.
- Barin, I.; and Knacke, O.: *Thermochemical Properties of Inorganic Substances*. Springer-Verlag, 1973.
- Barin, I.; Knacke, O.; and Kubaschewski, O.: *Thermochemical Properties of Inorganic Substances (Supplement)*, Springer-Verlag, 1977.
- Costello, J.A.; and Tressler, R.E.: Oxidation Kinetics of Silicon Carbide Crystals and Ceramics: I, In Dry Oxygen. *J. Am. Ceram. Soc.*, vol. 69, no. 9, 1986, pp. 674-681.
- Du, H., et al.: Oxidation Studies of Crystalline CVD Silicon Nitride. *J. Electrochem. Soc.*, vol. 136, no. 5, 1989, pp. 1527-1536.
- Schlichting, J.: High Temperature Oxidation of Disilicides in the System MoSi₂/TiSi₂. *Ceramurgia Int.*, vol. 4, no. 4, 1978, pp. 162-166.
- Hirai, T.; Niihara, K.; and Goto, T.: Oxidation of CVD Si₃N₄ at 1550° to 1650 °C. *J. Am. Ceram. Soc.*, vol. 63, no. 7-8, 1980, pp. 419-424.
- Narushima, T.; Goto, T.; and Hirai, T.: High-Temperature Passive Oxidation of Chemically Vapor Deposited Silicon Carbide. *J. Am. Ceram. Soc.*, vol. 72, no. 8, Aug. 1989, pp. 1386-1390.
- Saunders, W.A.; and Probst, H.B.: Evaluation of Oxidation Resistant Nonmetallic Materials at 1204 °C (2200 °F) in a Mach 1 Burner. NASA TN D-6890, 1972.
- Maeda, et al.: Oxidation Behavior of Silicon Nitride Under Cyclic and Static Conditions. *Ceramics Int.*, vol. 15, no. 4, 1989, pp. 247-253.
- Andrews, P.; and Riley, F.: Oxidation of Silicon Nitride During High Temperature Thermal Cycling, vol. 89, no. 6, *British Ceramic Transactions and Journal*, Institute of Ceramics Proceedings 46.
- Kingery, W.D.; Bowen, H.K.; and Uhlmann, D.R.: *Introduction to Ceramics*. 2nd ed., Wiley, New York, 1976, p. 274.
- Deal, B.E.; and Grove, A.S.: General Relationship for the Thermal Oxidation of Silicon. *J. Appl. Phys.*, vol. 36, no. 12, 1965, pp. 3770-3778.
- Jorgenson, P.J.; Wadsworth, M.E.; and Cutler, I.B.: Effects of Water Vapor on the Oxidation of SiC. *J. Am. Ceram. Soc.*, vol. 44, no. 6, 1961, pp. 258-261.
- Narushima, T., et al.: High-Temperature Oxidation of Chemically Vapor-Deposited Silicon Carbide in Wet Oxygen at 1823 to 1923 °K. *J. Am. Ceram. Soc.*, vol. 73, no. 12, 1990, pp. 3580-3584.
- Schlichting, J.: Oxygen Transport Through Silica Surface Layers on Silicon-Containing Ceramic Materials. *High Temp.-High Press.*, vol. 14, 1982, pp. 717-724.
- Thomas-Obgjuji, L.U.J.; and Smialek, J.L.: Oxide/Nitride Interface in Oxidized Silicon Nitride. Paper no. 515, *Electrochemical Society Meeting*, Washington, DC, May 6, 1991.
- Boch, P., et al.: Sintering, Oxidation and Mechanical Properties of Hot Pressed Aluminum Nitride. *Cer. Int.*, vol. 8, no. 1, 1982, pp. 34-40.
- Sato, T., et al.: High Temperature Oxidation of Hot-Pressed Aluminum Nitride by Water Vapor. *J. Mater. Sci.*, vol. 22, no. 6, 1987, pp. 2277-2280.
- Cheng, M.C.; and Cutler, I.B.: Vaporization of Silica in Steam Atmospheres. *J. Am. Ceram. Soc.*, vol. 62, no. 11, 1979, pp. 593-596.
- Tedmon, C.S.: The Effect of Oxide Volatilization on the Oxidation Kinetics of Cr and Fe-Cr Alloys. *J. Electrochem. Soc.*, vol. 113, no. 8, 1966, pp. 766-768.
- Jacobson, N.S.; Lee, K.N.; and Fox, D.S.: Reactions of SiC and SiO₂ at Elevated Temperatures. in preparation for *J. Am. Ceram. Soc.*
- Misra, A.K.: Thermochemical Analysis of Chemical Processes Relevant to the Stability and Processing of SiC-Reinforced Si₃N₄ Composite. *Ceramic Engineering and Science Proceedings*, vol. 12, no. 7-8, July-Aug. 1991.
- Luthra, K.L.: Thermochemical Analysis of the Stability of Continuous SiC Fibers. *J. Am. Ceram. Soc.*, vol. 69, no. 10, 1986, pp. C-231 to C-233.
- Paule, R.C.: Mass Spectrometric Studies of Al₂O₃ Vaporization Processes. *High Temp. Sci.*, vol. 8, no. 3, 1976, pp. 257-266.
- Kashireninov, O.E.; Chervonnyi, A.D.; and Piven, V.A.: On the Detection and Thermodynamic Characteristics of AlO₂. *High Temp. Sci.*, vol. 15, no. 2-3, 1982, pp. 79-91.
- Jacobson, N.S.: Thermodynamic Properties of Some Metal Oxide-Zirconia Systems. NASA TM-102351, 1989.
- Parker, F.J.: Al₂TiO₅-ZrTiO₄-ZrO₂ Composites: A New Family of Low-Thermal-Expansion Ceramics. *J. Am. Ceram. Soc.*, vol. 73, no. 4, 1990, pp. 929-932.
- Levin, E.M.; and McMurdie, H.F.: *Phase Diagrams for Ceramists*, 1975 Supplement, American Ceramic Society, Columbus, OH, 1975.
- Roth, R.S.; Dennis, J.R.; and McMurdie, H.F.: Phase Diagram for Ceramists: *Am. Ceram. Soc.*, vol. VI, 1987, p. 183.
- Sato, T.; Endo, T.; and Shimada, M.: Degradation of Mechanical Properties of Zirconia Ceramics by Low Temperature Annealing. *Jirukonia Seranikkusu*, vol. 10, 1989, pp. 157-174.
- Misra, A.K.: Thermodynamic Analysis of Chemical Stability of Ceramic Materials in Hydrogen-Containing Atmospheres at High Temperatures. NASA CR-4271, 1990.
- Jaskowiak, M.H., et al.: Effects of ZrO₂ Interfacial Coatings in Al₂O₃/Al₂O₃ Composites. *HITEMP Review 1990*, NASA CP-10051, 1990, pp. 60-1 to 60-12.
- Norkitis, M.E.; and Hellmann, J.R.: Sapphire Fiber-Reinforced Polycrystalline Alumina Composites. *HITEMP Review 1990*, NASA CP-10051, 1990, pp. 61-1 to 61-6.
- Touloukian, Y.S., et al.: *Thermal Expansion Nonmetallic Solids*. Plenum, New York, 1977.

50. Price, J.R.; and van Roode, M.: Corrosion Resistant Coating for Silicon Carbide. *Corrosion and Corrosive Degradation of Ceramics (Ceramic Transactions, Vol. 10)*, R.E. Tressler and M.J. McNallan, eds., American Ceramic Society, 1989, pp. 469-493.

REPORT DOCUMENTATION PAGE			Form Approved OMB No. 0704-0188	
Public reporting burden for this collection of information is estimated to average 1 hour per response, including the time for reviewing instructions, searching existing data sources, gathering and maintaining the data needed, and completing and reviewing the collection of information. Send comments regarding this burden estimate or any other aspect of this collection of information, including suggestions for reducing this burden, to Washington Headquarters Services, Directorate for Information Operations and Reports, 1215 Jefferson Davis Highway, Suite 1204, Arlington, VA 22202-4302, and to the Office of Management and Budget, Paperwork Reduction Project (0704-0188), Washington, DC 20503.				
1. AGENCY USE ONLY (Leave blank)	2. REPORT DATE January 1992	3. REPORT TYPE AND DATES COVERED Technical Paper		
4. TITLE AND SUBTITLE High-Temperature Durability Considerations for HSCT Combustor			5. FUNDING NUMBERS WU-505-63-20	
6. AUTHOR(S) Nathan S. Jacobson				
7. PERFORMING ORGANIZATION NAME(S) AND ADDRESS(ES) National Aeronautics and Space Administration Lewis Research Center Cleveland, Ohio 44135 - 3191			8. PERFORMING ORGANIZATION REPORT NUMBER E-6343	
9. SPONSORING/MONITORING AGENCY NAMES(S) AND ADDRESS(ES) National Aeronautics and Space Administration Washington, D.C. 20546-0001			10. SPONSORING/MONITORING AGENCY REPORT NUMBER NASA TP-3162	
11. SUPPLEMENTARY NOTES Responsible person, Nathan S. Jacobson, (216) 433-5498.				
12a. DISTRIBUTION/AVAILABILITY STATEMENT Unclassified - Unlimited Subject Category 27			12b. DISTRIBUTION CODE	
13. ABSTRACT (Maximum 200 words) The novel combustor designs for the High Speed Civil Transport will require high-temperature materials with long-term environmental stability. Higher liner temperatures than in conventional combustors and the need for reduced weight necessitate the use of advanced ceramic-matrix composites. In this report the combustor environment is defined at the current state of design, the major degradation routes are discussed for each candidate ceramic material, and where possible, the maximum use temperatures are defined for these candidate ceramics.				
14. SUBJECT TERMS Ceramics; High temperature environments; Volatility; Oxidation; Chemical reactions; Combustion			15. NUMBER OF PAGES 20	
			16. PRICE CODE A03	
17. SECURITY CLASSIFICATION OF REPORT Unclassified	18. SECURITY CLASSIFICATION OF THIS PAGE Unclassified	19. SECURITY CLASSIFICATION OF ABSTRACT	20. LIMITATION OF ABSTRACT	

